

# Mechanisms underlying diurnal variations in the canopy spectral reflectance of winter wheat in the jointing stage

Yinghao Lin<sup>1,2</sup>, Huaifei Shen<sup>3</sup>, Qingjiu Tian<sup>1,\*</sup>, Xingfa Gu<sup>4</sup>, Ranran Yang<sup>1</sup> and Baojun Qiao<sup>2</sup>

<sup>1</sup>International Institute for Earth System Science, School of Geographic and Oceanographic Sciences, Nanjing University, No.163, Xianlin Avenue, Qixia District, Nanjing, China, 210023

<sup>2</sup>Henan Key Laboratory of Big Data Analysis and Processing, School of Computer and Information Engineering, Henan University, Jinming Avenue, Longting District, Kaifeng, China 475004

<sup>3</sup>School of Urban and Rural Planning and Landscape Architecture, Xuchang University, No. 88, Bayi Road, Weidu District, Xuchang, China 461000

<sup>4</sup>Aerospace Information Research Institute, Institute of Remote Sensing and Digital Earth, Chinese Academy of Sciences, No. 20, Datun Road, Chaoyang District, Beijing, China 100094

**Information regarding diurnal variations in vegetation canopy spectra and vegetation indices (VIs) is necessary for plant growth modelling. We analysed the diurnal change characteristics of canopy spectral reflectance and VIs of winter wheat in the jointing stage based on field-measured and simulated spectral data. The visible–near infrared reflectance showed a double peak followed by a deep trough. The double-peak period occurred from 11:00 to 13:00 h (UTC + 8), and reflectance fluctuated greatly during this period. This change was attributed to midday depression of photosynthesis caused by stomatal closure induced by strong solar radiation. We found that the vegetation canopy reflectance was mainly affected by photosynthesis rate, solar irradiation intensity and surplus leaf water content. All selected VIs (normalized difference vegetation index (NDVI), photochemical reflectance index (PRI), water band index (WBI) and mSR705) exhibited distinct intraday variations, and VIs during the double-peak period tended to fluctuate strongly or decrease (NDVI, WBI and mSR705). Thus, field measurements during the double-peak period are not recommended for winter wheat in the jointing stage, with the exception of carotenoid content monitoring. A comparison of VIs showed that  $S_{VNIR}$ , NDVI and mSR705 were more sensitive to canopy structure in comparison with PRI and WBI.**

**Keywords:** Canopy reflectance, diurnal variation, jointing stage, photosynthesis rate, winter wheat.

REMOTE sensing (RS) has several advantages over other modes of gathering information about the surface of the earth, including high speed, low cost, objectivity and a relatively large sensing area. As a result, RS has become

an important tool for vegetation monitoring<sup>1</sup>. Vegetation spectral characteristics are determined by internal factors of vegetation such as canopy structure and major biochemical components, as well as external environmental factors such as atmospheric and soil conditions. Therefore, the RS vegetation spectra can be utilized to gather information regarding coverage percentages<sup>2</sup>, crop varieties and planting densities<sup>3</sup>, fertilizer levels<sup>4</sup>, moisture conditions<sup>5</sup> and soil types<sup>6</sup>.

Previous studies utilizing time-series RS data for vegetation monitoring have mainly focused on variation as a function of growth stage<sup>7</sup>. Few studies have assessed diurnal changes in the spectral reflectance and vegetation indices (VIs) of the vegetation canopy. Li *et al.*<sup>8</sup> reported that the diurnal normalized difference vegetation index (NDVI) of winter wheat on 22 May 2006 followed a U-shaped function. Möttus *et al.*<sup>9</sup> found that the photochemical reflectance index (PRI) of Scots pine needles exposed to direct radiation had a distinct diurnal cycle with constant or slightly increasing values before noon and a daily minimum in the afternoon. Guo *et al.*<sup>10</sup> confirmed that the canopy spectral reflectance of winter wheat varies as a function of solar angle, by comparing field-measured data under clear and cloudy sky conditions. Therefore, analysis of the causes of diurnal variation of vegetation canopy spectral reflectance and the ways in which VIs are affected by intraday phenology is necessary to improve the stability of remote sensing retrieval algorithms<sup>11</sup>. Vegetation canopy hyperspectral data were obtained continuously at two sample points throughout the day using ASD HandHeld 2 spectroradiometers (Analytical Spectral Devices, Boulder, Co, USA). Simulated spectral data were obtained using the PROSAIL model with input vegetation parameters set according to the crop conditions and solar angles at each observation time. The results of this study provide a theo-

\*For correspondence. (e-mail: tianqj@nju.edu.cn)

retical reference for phase selection in field-observation campaigns and the determination of vegetation indices using multi-source RS data.

## Materials and methods

### Data

*Measured hyperspectral reflectance data from field experiments:* The test site for the study was located in Shui-kou town (Laian county) in China's Yangtze River Basin (32°17'34.76"N, 118°27'36.42"E). The test site had a north subtropical humid monsoon climate. In April 2015, the monthly average temperature was 14.8°C, monthly average rainfall was 79.1 mm and total number of hours of sunshine per month was 171.8 h.

Hyperspectral reflectance data at the canopy level were collected at 15 min intervals under clear sky conditions between 9:30 and 15:00 h (UTC + 8) on 17 April 2015 using an ASD HandHeld 2 spectroradiometer fitted with a 25° field-of-view fibre-optic adaptor. The ASD HandHeld 2 was used to sample light with a wavelength between 325 and 1075 nm (spectral resolution <3.0 nm at 700 nm), and data were resampled to 1 nm spacing automatically. The sensor was placed directly above the target canopy and aimed straight down (Figure 1).

Two fixed sample points, *A* and *B*, were utilized for the collection of winter wheat canopy hyperspectral reflectance data. Each sample point was a circular area with a radius of approximately 0.2 m. Points *A* and *B* had different canopy structures; plants at point *A* were of a similar height, whereas those at point *B* had different heights. Data were collected in the jointing stage of growth. The crops appeared to be growing well at both sampling points and completely covered the ground.

ViewSpecPro was used to preprocess the measured hyperspectral data, after which MATLAB was used to apply a Savitzky–Golay filter to reduce noise and mixed signals<sup>12</sup>. Finally, Excel was used to obtain first-order derivatives, calculate correlation coefficients and extract vegetation indices.

*Simulation of reflectance data using the PROSAIL model:* The PROSAIL radiative transfer model can approximately

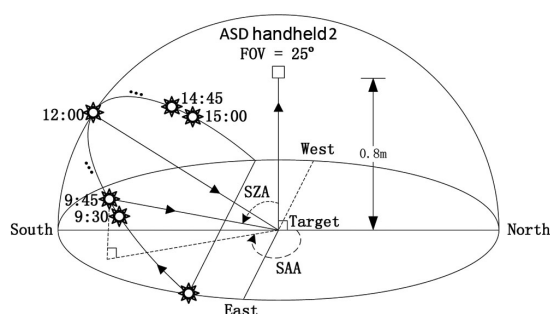


**Figure 1.** Diagrammatic representation of the measurement method.

simulate the spectral reflectance data of a vegetation canopy within the 400–2500 nm band range<sup>13</sup>. The sensitivity of each parameter was considered<sup>14</sup>, after which a range of input parameters was selected on the basis of their sensitivity, field observations, and the extant literature. Finally, initial values of each parameter were estimated and adjusted<sup>15</sup>. Table 1 shows the main input parameters. To reduce the number of influencing factors, only the solar zenith angle (SZA) was calculated based on the local time of observations; all other parameters remained unchanged during the observation period. Therefore, the simulation reflectance changed exclusively in response to changes in the solar angle. A single set of simulation data was used in the following analysis because points *A* and *B* were located close together. Figure 2 shows the changes in SZA on 17 April 2015.

### Selection of vegetation indices

In this study, diurnal variations in an array of VIs were comprehensively analysed (Table 2). The selected VIs included NDVI<sup>16</sup>, PRI<sup>17</sup>, water band index (WBI)<sup>18</sup> and chlorophyll content index mSR705 (mSR, modified simple ratio)<sup>19</sup>. We also calculated the area of reflectance in visible–near infrared (VNIR; 400–900 nm),  $S_{VNIR}$ , to gauge diurnal variations in the winter wheat canopy spectrum.

## Results

During the observation period, both field-measured and simulated data exhibited characteristics typical of a vegetation spectrum, and these characteristics were reasonably similar at different observation times. Specifically, all spectra presented two absorption peaks in the blue–violet and red regions, a strong reflection peak in the green region, and a high reflection platform in the region beyond 680 nm.

### Double-peak characteristic of $S_{VNIR}$

Diurnal changes in  $S_{VNIR}$  calculated from the field-measured data showed fluctuations (Figure 3). The observation period can be divided into three categories in terms

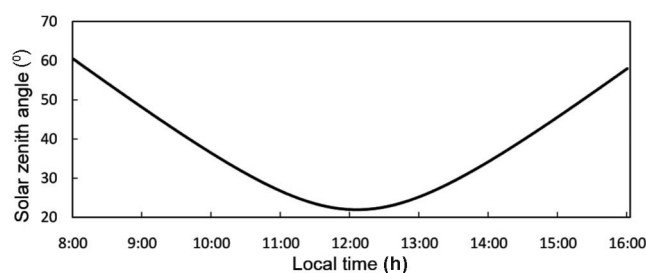


**Figure 2.** Diurnal variations in the solar zenith angle on 17 April 2015.

**Table 1.** Parameters and variables used to simulate canopy reflectance using PROSAIL

Model	Symbol	Values	Quantity
Prospect	$C_{ab}$	35 $\mu\text{g cm}^{-2}$	Chlorophyll $a + b$ content
	$C_w$	0.016 cm	Equivalent water thickness
	$C_m$	0.004 $\text{g cm}^{-2}$	Dry matter content
	$C_{bp}$	8 $\mu\text{g cm}^{-2}$	Brown pigment content
	$N$	1.5	Leaf structure parameter
Sail	LAI	3.5	Leaf area index
	ALA	70	Average leaf angle
	$\rho_s$	1	Soil reflectance (assumed Lambertian or not)
	SKYL	0.25	Ratio of diffuse to total incident radiation
	SL	0.2	Hot-spot parameter
	SZA	Corresponds to observation local time ( $^\circ$ ), see Figure 2	Solar zenith angle
	VZA	$0^\circ$	Viewing zenith angle
	RAA	$180^\circ$	Relative azimuth angle

**Table 2.** Overview of the selected vegetation indices

Symbol	Evaluation expression	Symbol	Evaluation expression
$S_{VNIR}$	SUM (R400 to R900)	WBI	R900/R970
NDVI	$(R800 - R680)/(R800 + R680)$	mSR705	$(R750 - R445)/(R705 + R445)$
PRI	$(R531 - R570)/(R531 + R570)$		

R400 is the vegetation canopy reflectance at wavelength 400 nm,  $R^*$  represents the vegetation canopy reflectance at wavelength \*(unit: nm).

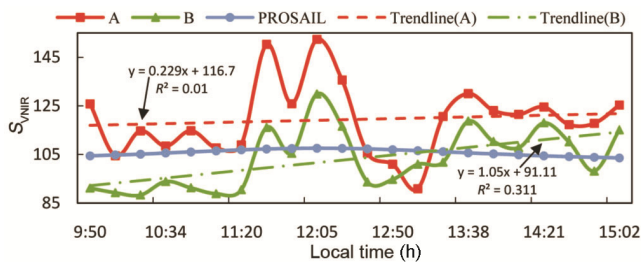


**Figure 3.** Diurnal variations in  $S_{VNIR}$ .  $S_{VNIR}$ , Reflectance area from 400 to 900 nm; A,  $S_{VNIR}$  calculated with field-measured data from point A. B,  $S_{VNIR}$  calculated with field-measured data from point B. PROSAIL,  $S_{VNIR}$  calculated with simulated data from the PROSAIL model. Trendline (A), Linear fitted curve of  $S_{VNIR}$  from point A. Trendline (B), Linear fitted curve of  $S_{VNIR}$  from point B.

of amplitude: 9:30–11:00 h, 13:00–15:00 h and 11:00–13:00 h. The former two periods had smaller absolute deviations, but  $S_{VNIR}$  value in the afternoon (13:00–15:00 h) was larger than that in the morning (9:30–11:00 h). The 11:00–13:00 h period is the double-peak period, in which two peak values occur at 11:40 and 12:00 h and two trough values occur at 11:59 and 13:00 h. The  $S_{VNIR}$  calculated with simulated data changed smoothly during the observation period and showed no fluctuations. There were two differences between the  $S_{VNIR}$  values calculated with the field-measured data. First, the two peak values of point A were nearly equal, but those of point B differed. Second, the minimum value of the second trough of point A occurred

around 13:00 h, whereas that of point B occurred at 12:40 h.

### Diurnal variation in selected vegetation indices

All of the selected VIs were calculated with field-measured data from points A and B, as well as with simulated data from the PROSAIL model (Figure 4). Generally, each VI exhibited distinct intraday variation, and there were relatively minor differences between points A and B. During the double-peak period, VIs usually fluctuated strongly or exhibited smaller values, as was observed for NDVI, WBI and mSR705.

During the observation period, NDVI based on field-measured data showed fluctuations and reached a minimum value around noon, as reported in similar studies<sup>8</sup>. In contrast, NDVI based on simulated data approximated a smooth curve (Figure 4a). Diurnal changes in PRI of points A and B showed a steadily fluctuating upward trend, and the rate of this trend increased over time (Figure 4b). These results indicate that the light utility efficiency of winter wheat increased over time, and there was no saturation during the observation period. PRI based on simulated data changed slightly over time with a minimum around noon. Diurnal changes in WBI of points A and B generally showed a fluctuating upward trend, although stable fluctuation was observed from 11:49 to 13:50 h (Figure 4c). The maximum WBI of point A (at 13:04 h) was beyond the distribution range of general

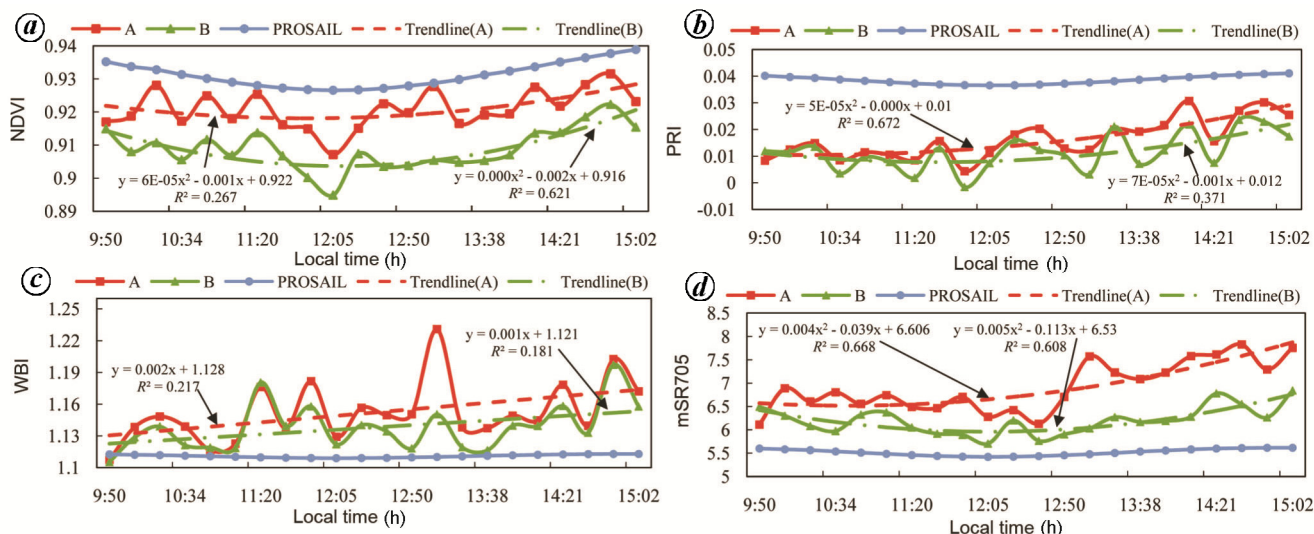


**Figure 4.** Diurnal variations in the selected VIs. For (a) NDVI; (b) PRI; (c) WBI and (d) mSR705. A, VI calculated with field-measured data from point A. B, VI calculated with field-measured data from point B. PROSAIL, VI calculated with simulated data from the PROSAIL model. Trendline (A), Binomial fitted curve of VI from point A. Trendline (B), Binomial fitted curve of VI from point B.

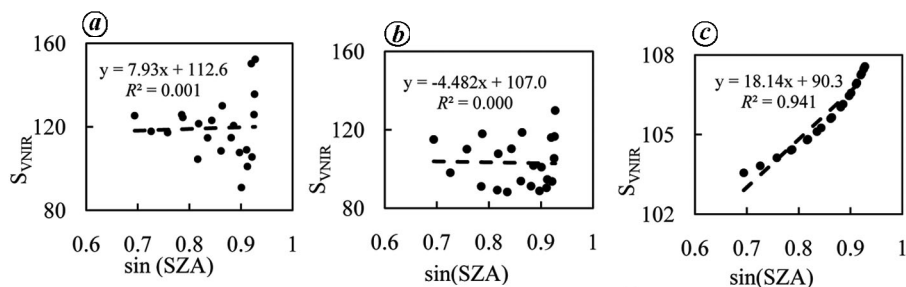


**Figure 5.** Relationship between  $\sin(SZA)$  and  $S_{VNIR}$  for (a) field-measured data from point A, (b) field-measured data from point B and (c) simulated data from the PROSAIL model.

green vegetation (0.8–1.2); further discussion on this is omitted for brevity. WBI based on simulated data exhibited a small trough around noon. During the observation period, the mSR705 values of field-measured data showed fluctuations (Figure 4d). Even through the binomial fitted curves for mSR705 of points A and B showed different trends, lower values of mSR705 both appeared around noon. The mSR705 values based on simulated data showed a slight trough, which also occurred around noon.

*Mechanisms underlying diurnal variation of the winter wheat canopy spectrum*

*Effect of solar zenith angle on winter wheat canopy reflectance:* The diurnal changes in VIs based on simulated data had minimum or maximum values around noon, and their curves were similar in shape to the sine function. Therefore, we established the linear relationship between spectral variables (taking  $S_{VNIR}$  as an example) and  $\sin(SZA)$  (Figure 5).

The coefficient of determination ( $R^2$ ) of the linear relationship between  $S_{VNIR}$  and  $\sin(SZA)$  of the simulated

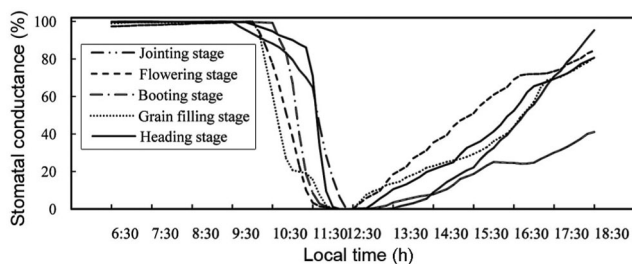
data was very high (0.941). Whereas  $R^2$  of the linear relationship between  $S_{VNIR}$  and  $\sin(SZA)$  of field-measured data was close to zero, and  $S_{VNIR}$  distribution became more widely dispersed as the  $\sin(SZA)$  value increased (Figure 5a and b). These results illustrate that, in addition to SZA, other factors strongly influenced the field-measured spectrum, including environmental factors such as temperature and the soil-to-vegetation ratio, as well as internal factors such as pigment content and leaf water content.

*Effect of physiological characteristics of vegetation:* It has hitherto been reported that vegetation can respond to excessive incident light intensity by stomatal closing, which is known as midday depression of photosynthesis<sup>20</sup>. NDVI and PRI have been reported to be closely related to photosynthesis<sup>21</sup> and their minimum recorded values around noon could directly indicate depression of photosynthesis. The factors contributing to this midday depression in photosynthesis include water conditions<sup>22</sup>, stomatal conductance<sup>23</sup>, and the accumulation and transportation of photosynthetic products<sup>24</sup>. Of particular note, Yu and Liu<sup>24</sup> monitored the stomatal conductance of wheat during different growth stages (Figure 6), which

**Table 3.** Diurnal variations in the selected vegetation indices based on field-measured and simulated data (fitted curves)

VIs	Point A	Point B	Simulated data	VIs	Point A	Point B	Simulated data
$S_{VNIR}$	DP, I*	DP, I**	P*	WBI	I**	I**	T*
NDVI	ST*	ST**	ST**	mSR705	I**	ST**	T**
PRI	I**	I**	T*				

VIs, Vegetation indices; DP, Double-peak characteristic; T, had a single minimum value; P, the blue curve in Figure 3 had a single week peak, that is to say, it had a single maximum value; I, Increase; D, Decrease; C, Constant; S, Minimum or maximum value occurred around noon; L, Minimum or maximum value occurred before noon; R, Minimum or maximum value occurred after noon. \* and \*\*Indicate that the difference between maximum and minimum of the fitted curve is smaller than 0.5 major  $y$ -axis units and larger than 0.5 major  $y$ -axis units respectively.

**Figure 6.** Diurnal variations in stomatal conductance in wheat at different growth stages<sup>24</sup>.

revealed that the stomata completely closed around noon under clear day conditions from the jointing stage to the grain-filling stage.

Figure 3 shows that the double-peak period is followed by a deep trough around 13:00 h, when stomatal conductance is close to 0 (Figure 6). At 13:00 h, both NDVI and PRI show lower values and WBI shows a larger value. We can speculate that the leaf water content exceeded photosynthetic demand, resulting in relatively high leaf water content. The role of water in the darkening and redistribution of illumination on objects has been described literature<sup>25</sup>. As the day proceeds beyond 13:00 h, stomatal conductance gradually increases and photosynthesis intensifies. These changes reduce leaf water content and canopy reflectance rebounds to a high value.

## Discussion

Diurnal changes in  $S_{VNIR}$  calculated from field-measured data showed fluctuations and a double-peak followed by a deep trough (Figure 3). The VIs at both sampling points exhibited similar diurnal trends, despite subtle dissimilarities caused by canopy differences. This finding indicates that the observed diurnal variations are stable. However, the diurnal variations of canopy spectral reflectance and VIs of winter wheat change along with the growth stage<sup>8</sup>. Thus, the extent to which the double-peak characteristic of diurnal variation in canopy spectral reflectance occurs under different conditions should be determined. In addition,

variations in canopy spectral reflectance are clearly time-sensitive; therefore, more time intervals and more sample points need to be assessed to show the timescale effect of the double-peak characteristic.

The VIs based on field-measured and simulated data exhibited differential fitted trends (Table 3). As already noted, points A and B were exposed to homogeneous growing environments. We can therefore conclude that these VI differences were mainly caused by differences in the canopy structure. The  $S_{VNIR}$ , NDVI, and mSR705m at point A exhibited large numerical differences compared to those at point B, and those calculated using simulated data, which indicates that these indices are relatively sensitive to canopy structure. PRI and WBI tended to exhibit relatively small differences, indicating that these indices were relatively insensitive to canopy structure.

In this study, we found that the deep trough that occurs after the double-peak period is caused by midday photosynthesis depression mediated by closing of the stomata due to the high radiation intensity around noon. To further analyse the mechanisms underlying the double-peak characteristic in the canopy spectral reflectance of winter wheat, synchronous and detailed data for transpiration, respiration and photosynthesis in the vegetation canopy must be analysed.

## Conclusion

In this study, we analysed diurnal variations in the vegetation canopy spectral reflectance and VIs of winter wheat in the jointing stage. We have defined an explicit relationship between canopy spectral reflectance of winter wheat and midday depression of photosynthesis. Results show that  $S_{VNIR}$  computed from field-measured data displayed fluctuations; a double-peak followed by a deep trough, and reflectance in the afternoon is higher than that in the morning. Diurnal variations in NDVI follow a U-shape with fluctuations, while PRI, WBI, and mSR705 present a steadily fluctuating upward trend, with mSR705 exhibiting a relatively low value in the double-peak period. Generally speaking, the field-measured

winter wheat canopy spectrum is impacted by changes in vegetation photosynthesis activity related to changes in surplus leaf water content; where vegetation photosynthesis is more active, there is less surplus leaf water content and higher canopy spectral reflectance. This study provides an important insight into the relationship between photosynthesis and vegetation spectrum of winter wheat, as well as the mechanisms underlying this link, based on analysis of field-measured and simulated diurnal variations in VIs and spectral reflectance.

*Conflicts of interest:* The authors declare no conflict of interest.

1. Sui, J. *et al.*, Winter wheat production estimation based on environmental stress factors from satellite observations. *Remote Sensing*, 2018, **10**, 962.
2. Huete, A., Jackson, R. and Post, D., Spectral response of a plant canopy with different soil backgrounds. *Remote Sensing Environ.*, 1985, **17**, 37–53.
3. Hatfield, J. L. and Prueger, J. H., Value of using different vegetative indices to quantify agricultural crop characteristics at different growth stages under varying management practices. *Remote Sensing*, 2010, **2**, 562–578.
4. Quemada, M., Gabriel, J. L. and Zarco-Tejada, P., Airborne hyperspectral images and ground-level optical sensors as assessment tools for maize nitrogen fertilization. *Remote Sensing*, 2014, **6**, 2940–2962.
5. Cosh, M. *et al.*, Downscaling of surface soil moisture retrieval by combining MODIS/landsat and *in situ* measurements. *Remote Sensing*, 2018, **10**, 210.
6. Ding, Y., Zheng, X., Zhao, K., Xin, X. and Liu, H., Quantifying the impact of NDVI<sub>soil</sub> determination methods and NDVI<sub>soil</sub> variability on the estimation of fractional vegetation cover in northeast China. *Remote Sensing*, 2016, **8**, 29.
7. Huang, S. *et al.*, Potential of rapid eye and world view-2 satellite data for improving rice nitrogen status monitoring at different growth stages. *Remote Sens.*, 2017, **9**, 227.
8. Li, S. *et al.*, Correlation between spectral characteristics and diurnal CO<sub>2</sub> budget of winter wheat field on Loess plateau. *Chin. J. Appl. Ecol.*, 2008, **19**, 2408–2413.
9. Möttus, M. *et al.*, Measurement of diurnal variation in needle PRI and shoot photosynthesis in a boreal forest. *Remote Sensing*, 2018, **10**, 1–14.
10. Guo, J., Wang, Q., Tong, Y., Fei, D. and Liu, J., Effect of solar radiation intensity and observation angle on canopy reflectance hyperspectra for winter wheat. *Nongye Gongcheng Xuebao/Trans. Chinese Soc. Agric. Eng.*, 2016, **32**, 157–163.
11. Sticksel, E., Schächtl, J., Huber, G., Liebler, J. and Maidl, F. X., Diurnal variation in hyperspectral vegetation indices related to winter wheat biomass formation. *Precis. Agric.*, 2004, **5**, 509–520.
12. Chen, J., Jönsson, P., Tamura, M., Gu, Z., Matsushita, B. and Eklundh, L., A simple method for reconstructing a high-quality NDVI time-series data set based on the Savitzky-Golay filter. *Remote Sensing Environ.*, 2004, **91**, 332–344.
13. Jacquemoud, S. *et al.*, PROSPECT + SAIL models: a review of use for vegetation characterization. *Remote Sensing Environ.*, 2009, **113**, S56–S66.
14. Dian, Y. and Fang, S., Simulation analysis of vegetation TOA reflectance based on coupled leaf–canopy–atmosphere radiative transfer model. *Remote Sensing Land Resour.*, 2013, **25**, 30–37.
15. Hosgood, B., Jacquemoud, S., Andreoli, G., Verdebout, J., Pedrini, G., and Schmuck, G., Leaf Optical Properties EXperiment 93 (LOPEX93). Eur. Comm. Jt. Res. Centre, Inst. Remote Sens. Appl. Rep. EUR 16095 EN, 1994.
16. Rouse, J. W., Hass, R. H., Schell, J. A. and Deering, D. W., Monitoring vegetation systems in the great plains with ERTS. In *Third Earth Resour. Technol. Satell. Symp.*, 1973, vol. 1, pp. 309–317.
17. Gamon, J. A., Peñuelas, J. and Field, C. B., A narrow-waveband spectral index that tracks diurnal changes in photosynthetic efficiency. *Remote Sensing Environ.*, 1992, **41**, 35–44.
18. Penuelas, J., Pinol, J., Ogaya, R. and Filella, I., Estimation of plant water concentration by the reflectance water index WI (R900/R970). *Int. J. Remote Sensing*, 1997, **18**, 2869–2875.
19. Sims, D. A. and Gamon, J. A., Relationships between leaf pigment content and spectral reflectance across a wide range of species, leaf structures and developmental stages. *Remote Sensing Environ.*, 2002, **81**, 337–354.
20. Prasad, A. K., Chai, L., Singh, R. P. and Kafatos, M., Crop yield estimation model for Iowa using remote sensing and surface parameters. *Int. J. Appl. Earth Obs. Geoinf.*, 2006, **8**, 26–33.
21. Gamon, J. A., Kovalchuck, O., Wong, C. Y. S., Harris, A. and Garrity, S. R., Monitoring seasonal and diurnal changes in photosynthetic pigments with automated PRI and NDVI sensors. *Biogeosciences*, 2015, **12**, 4149–4159.
22. Sawada, S. I., An ecophysiological analysis of the difference between the growth rates of young wheat seedlings grown in various seasons. *J. Fac. Sci. Univ. Tokyo III*, 1970, **10**, 233–263.
23. Maskell, E. J., Experimental researches on vegetable assimilation and respiration. XVII – The diurnal rhythm of assimilation in leaves of cherry laural at ‘limiting’ concentrations of carbon dioxide. *Proc. R. Soc. London Ser. B*, 1928, **102**, 467–487.
24. Yu, Y. and Liu, T., Study of the ecology of photo-effect on the plants I. Cause of Midnap in the wheat. *Acta Phytophysiol. Sin.*, 1985, **5**, 336–342.
25. Tian, J. and Philpot, W. D., Soil directional (biconical) reflectance in the principal plane with varied illumination angle under dry and saturated conditions. *Opt. Express*, 2018, **26**, 23883–23897.

ACKNOWLEDGEMENTS. This work was supported by the National Natural Science Foundation of China (41771370), the Foundation of Xuchang University for Outstanding Young Backbone Teachers, the National Key R&D Program of China (2017YFD0600903), and the High-resolution Earth Observation Project of China (03-Y20A04-9001-17/18, 30-Y20A07-9003-17/18). We thank the anonymous reviewers for their constructive comments that helped improve the manuscript.

Received 6 March 2019; revised accepted 22 January 2020

doi: 10.18520/cs/v118/i9/1401-1406